

pubs.acs.org/acsapm Article

# Structure—Performance Relationships of Li-Ion Battery Fiber-Based Separators

Salvatore Luiso,\* Michael J. Petrecca, Austin H. Williams, Jerush Christopher, Orlin D. Velev, Behnam Pourdeyhimi, and Peter S. Fedkiw



Cite This: ACS Appl. Polym. Mater. 2022, 4, 3676-3686

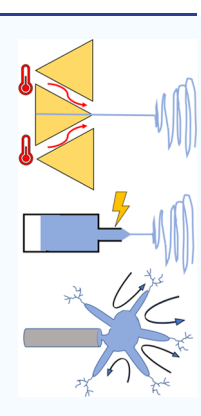


ACCESS

Metrics & More

Article Recommendations

ABSTRACT: Lithium-ion battery separators are receiving increased consideration from the scientific community. Many research efforts trend toward creating high-performance fiber-based battery separators with a small and uniform pore size to maximize ionic conductivity and cell discharge capacity. Here, we show that not only the pore size but also the pore size distribution has an important effect on these electrochemical properties. In this work, we studied nonwoven membranes fabricated from a single polymer, poly(vinylidene fluoride) (PVDF), with different pore sizes and pore size distributions using three different techniques (meltblowing, electrospinning, and shear spinning). We evaluate their performance as separators in Li-ion cells. Although meltblowing is commonly employed to produce commercial microfibers/nanofibers, electrospinning has been studied mostly in the academic literature. Shear spinning is an emerging method to fabricate nanofibrous material where, for this study, the morphology of the resulting PVDF membranes may be controlled from fibrous-like to nano-sheet-like with subsequent effects on the electrochemical properties. We show that the smaller the pore size and the wider the pore size distribution, the higher are the electrolyte uptake and ionic conductivity of the mats, resulting in improved in-use discharge capacity and rate capability of Li/LiCoO<sub>2</sub> cells.



KEYWORDS: meltblown, electrospun, shear, PVDF, nonwoven, separator, batteries

# ■ INTRODUCTION

The separators for a lithium-ion battery (LIB) are an important component of the device, but their chemical and electrochemical properties have been a subject of limited investigation relative to the other cell constituents. The choice of materials and manufacturing processes for separators is the focus of most literature studies. 1-7 Several reports showed correlations between structural properties (e.g., pore size and thickness), electrochemical properties of the membranes (e.g., electrolyte uptake and ionic conductivity), and discharge capacity/rate capability of Li-ion cells assembled with these separators. 5,8-12 However, these were single-case studies, and few focused on understanding the role of the separator pore network and its effect on cell electrochemical properties. In this research, we focus on analyzing relationships between the pore structure of poly(vinylidene fluoride) (PVDF)-based separators made with different processes and their in-use electrochemical properties, such as discharge capacity and rate capability of a Li-ion cell.

The relationships between structural and electrochemical properties of battery separators have recently attracted the attention of the scientific community. Several studies have utilized phase separation to introduce a unique structure into Li-ion battery separators. Hierarchically structured separators, for example, were prepared by Luo et al. 13 through a solvent liberation method and by Liu et al. 14 through a reformed gel with direct post-solidation procedure. By exploiting the difference in solvent evaporation rates between N-methyl

pyrrolidone and acetone, both groups created separators with high porosity that yield an ionic conductivity of 3.27 mS/cm after electrolyte uptake. The authors claim that the inter-island and inner-bound structures of the separators they produced reduce capacity loss in a LiFePO<sub>4</sub>/Li cell. Ye et al. <sup>15</sup> fabricated separators with a highly dense and porous inter-particle chain structure from polyvinylidene fluoride-hexafluoropropylene. The rearrangement of the polymer chains after electrolyte uptake is reported to create a microstructure that decreases thermal shrinkage and improves electrochemical properties. Different separator morphologies, such as sponge-like material with an asymmetric distribution of pores, <sup>17</sup> may be obtained not only with solvent—nonsolvent interactions <sup>5,13,16</sup> but also by changing the process conditions used in the separator fabrication. <sup>7,12</sup>

Fabricating separators from microfibers and nanofibers is another way to control the structural properties of separators. Fibrous separators have been widely studied because their pore structure allows high electrolyte wettability, ionic conductivity, and cell cycling performance. 6,18,19 Nano-structured fibrous

Received: February 2, 2022 Accepted: April 14, 2022 Published: April 26, 2022





battery separators are attractive because of their controllable compositions and pore structures. A fibrous network forms an interconnected nano/microporous structure that provides both openness for enhanced lithium-ion transport and mechanical strength for cell assembly. Trends in creating a fibrous battery separator have largely sought to achieve a pore size and distribution similar to well-established microporous membranes, that is, small and uniform pore size. However, a few outlier studies 20-24 suggest that a small pore size and a high porosity (reported as responsible for improved cycling performance in nonwovens) do not capture the effect that the pore size distribution has on the electrochemical properties. For example, Lee et al.<sup>20</sup> reported the importance of correlating the separator pore structure to the cell electrochemical properties. The authors relate the ionic conductance and the rate capability (Li/LiMnO<sub>4</sub> cells) to the normalized Gurley number, 25 which in turn they relate to separator thickness and porosity. However, these correlations do not uniquely specify the electrochemical performance of fibrous-based separators, as other factors, such as pore size distribution, should be considered. Ye et al.<sup>21</sup> decorated the surface of electrospun polyimide nanofibers with polyaniline to create a three-dimensional hierarchical micro-/nano-architecture. The presence of the so-called polyaniline nanowires decreased the average pore size but also increased the electrolyte uptake, resulting in an improved conductivity and cell cycling performance. Sabetzadeh et al.<sup>22</sup> showed that improved battery performance can be achieved when a multiscale porosity of the separator is present. These researchers introduced nanoporosity by means of phase separation in electrospun fibers, which increased conductivity and in-use capacity retention in a Li(Ni<sub>1/3</sub>Co<sub>1/3</sub>Mn<sub>1/3</sub>)O<sub>2</sub>/Li cell. A wide pore size distribution is regarded as an improvement also by Jiang et al.,<sup>23</sup> who introduced TiO<sub>2</sub> nanotubes in a poly-(vinylpyrrolidone) matrix. After a treatment at 500 °C, the separator presented nano- and meso-pores with a broad size distribution, which improved ionic conductivity and cell cycling. A small average pore size is not sufficient to improve the electrochemical properties of LIB separators, and a broad pore distribution seems to have a beneficial effect. Zhai et al.<sup>24</sup> showed that a tri-layered poly(*m*-phenylene isophthalamide) (PMIA)/PVDF/PMIA composite separator with a mean pore size of 0.85  $\mu$ m (range 0.71-2.41  $\mu$ m) has superior conductivity, tensile strength, and cycling performance compared to single-layer PVDF (mean pore size of 2.50  $\mu$ m, range 2.09–3.18  $\mu$ m) or PMIA (mean pore size of 0.53  $\mu$ m, range  $0.51-0.57 \mu m$ ). A small mean pore size and a wide pore size distribution seem to be beneficial for a high-performance LIB separator.

In this work, we analyze membranes with different pore sizes and distributions that are fabricated with a single polymer, PVDF, using three different techniques (meltblowing, electrospinning, and shear spinning), and we evaluate their performance as separators in a Li/LiCoO<sub>2</sub> cell. Meltblowing is a process commonly employed for the production of commercial microfibers/nanofibers where the melted polymer is extruded through a die with fine capillaries, after which a jet of hot air impinges on the emerging polymer filaments to form fibrous webs. In previous work, we demonstrated the feasibility of meltblowing PVDF and using the resulting webs as a battery separator.<sup>7,12</sup> Electrospinning uses an electric field to drive polymer fibers out of solution and has been widely used as a method to prepare a variety of functional fibrous mem-

branes. 2,6,8,18,38 Shear spinning is a method to fabricate nanofibrous material in which a polymer solution is injected into a sheared nonsolvent flow to create particles of various morphologies.<sup>26-28</sup> In a previous study,<sup>5</sup> we showed that the morphology of PVDF membranes prepared by the shear spinning technique may be controlled from fibrous soft dendritic colloids (SDCs) to a nano-sheet (NS) structure, with subsequent effects on the electrochemical properties. Here, by using three different techniques, meltblowing, electrospinning, and shear-spinning, we fabricate PVDF Liion battery separators with varying fiber/pore diameters and pore size distributions. For a given processing technique, we adjusted the processing conditions to ensure that the main difference among the separators produced was the average fiber/pore diameter and size distribution. We demonstrate that smaller mean pore size and wider pore size distributions within each manufacturing technique results in increased electrolyte uptake, ionic conductivity, discharge capacity, and rate capability of the mats in Li/LiCoO<sub>2</sub> cells.

#### EXPERIMENTAL SECTION

**Meltblowing Process.** We used an experimental-grade PVDF Kynar resin RC 10,287 (Arkema, Inc). The resin has low molecular weight (MW) (15–100 kDa), a melt viscosity of 0.2 kP at 230 °C at a shear rate of  $100~\rm s^{-1}$ , and a 2.0 poly-dispersity index (PDI).  $^{12,29,30}$  After drying the resin overnight at 70 °C, we prepared meltblown mats using a 1.2 m Reifenhauser-Reicofil Meltblown pilot line at the Nonwovens Institute at NC State University.  $^{31}$  Based on our previous work,  $^{7,12}$  the temperatures of both the die and the impinging air jets were held at 240 °C and fibrous mats were fabricated at a basis weight (BW) of 40 g/m² with the following process variables (the designation M1, M2, and M3 are abbreviations for these conditions and referenced in the Results and Discussion section):

- 1 M1. Throughput =  $46 \text{ kg h}^{-1}$ , airflow =  $1100 \text{ m}^3 \text{ h}^{-1}$ , and dieto-collector distance (DCD) = 20 cm
- 2 M2. Throughput =  $11 \text{ kg h}^{-1}$ , airflow =  $1000 \text{ m}^3 \text{ h}^{-1}$ , and DCD = 15 cm.
- 3 M3. Throughput =  $36 \text{ kg h}^{-1}$ , airflow =  $1100 \text{ m}^3 \text{ h}^{-1}$ , and DCD = 15 cm

**Electrospinning Process.** PVDF Kynar resin 761 (MW = 300–400 kDa and PDI = 4.0) was obtained from Arkema and dissolved in a mixture of dimethylformamide and acetone (7:3 v/v) at 12 or 16% weight concentration. The polymer solution was loaded in a 10 mL syringe with a 22-gauge needle and placed on a precision syringe pump with a constant flow rate of 1.5 mL h<sup>-1</sup>. The nanofibers were collected on aluminum foil placed on an aluminum collector plate connected to the grounded electrode. We fabricated electrospun PVDF mats at room temperature and 55  $\pm$  5% relative humidity with the following process variables:

- 4 E1. PVDF concentration = 12 wt %, voltage = 15 kV, tip-to-collector distance (TCD) = 15 cm, and  $BW = 100 \text{ g/m}^2$ .
- 5 E2. PVDF % = 16 wt %, voltage = 15 kV, TCD = 15 cm, and BW =  $17 \text{ g/m}^2$ .
- 6 E3. PVDF % = 12 wt %, voltage = 20 kV, TCD = 10 cm, and BW = 150  $\rm g/m^2$

**Shear Spinning Precipitation Process.** We dissolved PVDF resin (Sigma-Aldrich, MW = 530 kDa and PDI = 2.0) in dimethyl sulfoxide (DMSO, Fisher Scientific) by heating at 110 °C for 24 h while stirring. After cooling, the PVDF solution was injected at a rate of 1 mL/s into the shear zone of a colloidal mill (IKA Magic Lab) set to 20,000 rpm and filled with 500 mL of ethanol, as discussed elsewhere. S,26-28 After centrifuging the resulting PVDF suspensions and recovering the solid, we re-suspended the particles in ethanol and repeated the centrifugation process five times to remove residual DMSO. The final suspension was filtered (0.45  $\mu$ m filter pore size) to form a membrane, and the resulting membranes were dried in an air

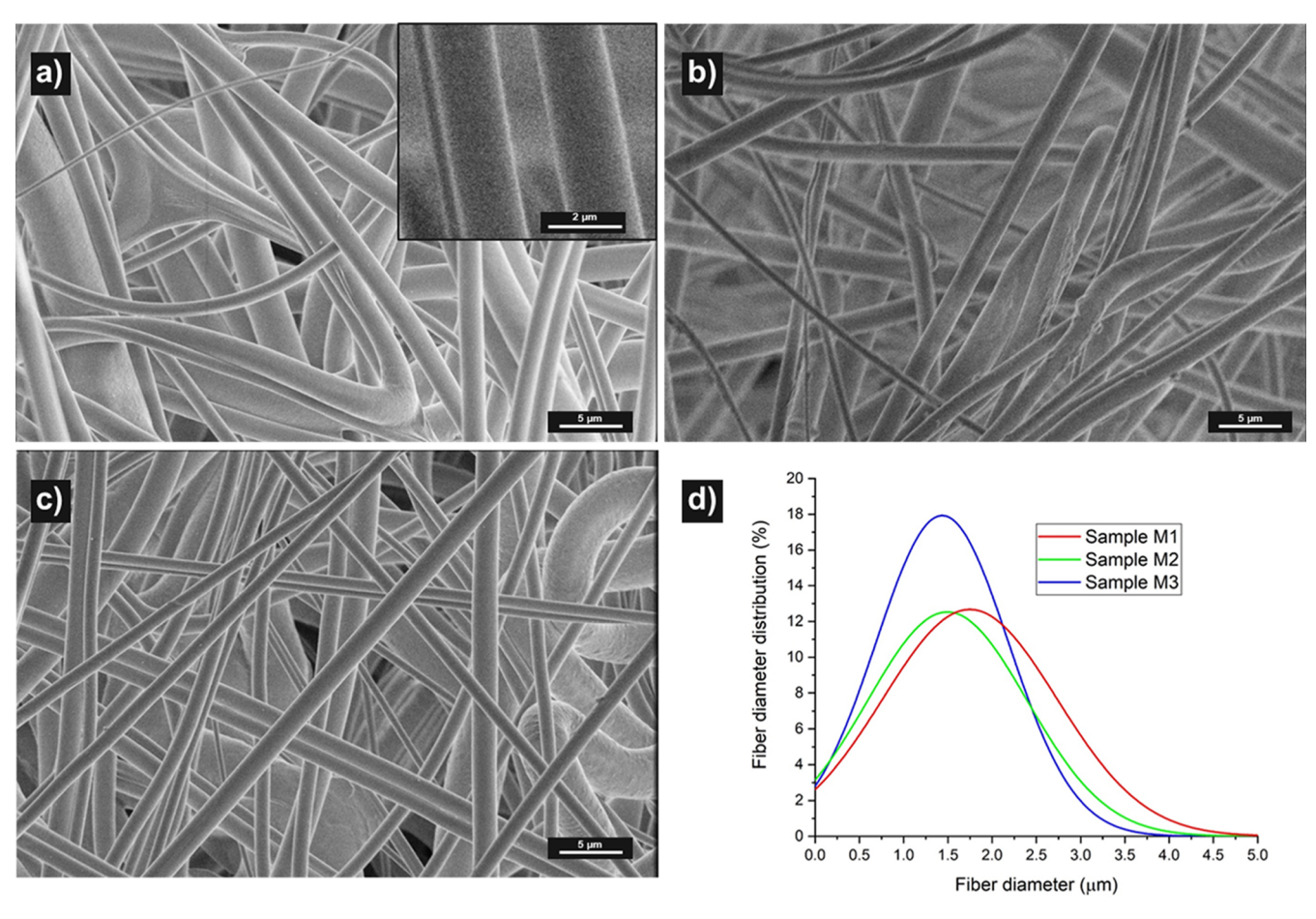


Figure 1. SEM images of meltblown PVDF separatorM1 (a, with inset at higher magnification), (b) M2, (c) M3, and (d) resulting fiber diameter distributions.

oven at 70  $^{\circ}$ C for 24 h. We produced SDC membranes with a BW of BW = 20 g/m² and with an initial PVDF concentration according to the schedule below.

- 7 S1. PVDF concentration in the injection solution = 5 wt % (fibers).
- 8 S2. PVDF % = 10 wt % [fiber nanosheets (NSs)].
- 9 S3. PVDF % = 12.5 wt % (NSs)

where a qualitative descriptor of the particle morphology is given in parenthesis.

**Microscopy.** A field emission scanning electron microscope (FEI Verios 460L) under a 2 kV accelerating voltage was used to examine the membrane morphology. The average fiber diameters were determined by using Fiji (ImageJ) software after taking at least 100 measurements from five different areas in each mat.

**Thickness and Solid Volume Percentage.** Mat thickness was measured with a Mitutoyo micrometer, and the solid volume percentage  $\epsilon_s$  was calculated using eq 1

$$\varepsilon_{\rm s} = \frac{W}{t\rho_{\rm fiber}} \times 100 \tag{1}$$

where W is the BW of the mat in g cm<sup>-2</sup>, t is the thickness in cm, and  $\rho_{\text{fiber}}$  is the density of the polymer (1.78 g cm<sup>-3</sup>).

**Capillary Flow Porosimetry.** The pore diameter was measured at the most constricted part of the pore (the bubble point diameter) and the pore diameter distribution was measured using an in-plane porometer (Porous Materials Inc). A highly wetting liquid (Salwick) with a known surface tension of 20.1 dyn cm<sup>-1</sup> was used to wet the mats, and no visible contact angle was detected (contact angle = 0°). The pore diameter was calculated with the Young–Laplace equation<sup>32</sup>  $D = 4\gamma_{L/G}\cos\theta/p$ , where p is the extrusion pressure in

MPa, D is the pore diameter in mm,  $\gamma_{\rm L/G}$  is the surface tension of Salwick (2.01  $\times$  10<sup>-5</sup> N/mm), and  $\theta$  is the contact angle of Salwick with the mat.

**Electrolyte Uptake.** All PVDF mats absorbed electrolyte quickly (<1 s), and electrolyte uptake was calculated with eq 2 by weighing the separators before and after soaking for 10 min in a 1 M LiPF $_6$  ethylene carbonate (EC)/dimethyl carbonate (DMC) 1:1 v/v mixture

electrolyte uptake = 
$$\frac{W_{\rm a} - W_{\rm b}}{W_{\rm b}} \times 100$$
 (2)

where  $W_{\rm b}$  and  $W_{\rm a}$  is the weight of the separator before and after soaking in the electrolyte, respectively. When soaked in electrolyte, the fibers swell and the mat undergoes volume expansion, which may vary with the density of its fibrous network. A non-uniform distribution of the fibrous morphology may cause significant variations in the uptake measurements. To reduce uncertainties and assess reproducibility, we removed the surface-bound electrolyte with wax paper and measured electrolyte uptake on at least five replicas.

**lonic Conductivity.** In an Argon-filled glovebox, 50  $\mu$ L of 1 M LiPF<sub>6</sub> in EC/DMC (1:1 v/v) was added to punched separators (15.9 mm diameter), which were then sandwiched between stainless-steel spacers and assembled in a CR2032 coin cell. Electrochemical impedance spectroscopy (EIS) measurements were performed with a Bio-Logic VMP3 16-Channel potentiostat. The EIS frequency ranged from 500 kHz to 1 Hz with an amplitude of 10 mV. The ionic conductivity,  $\sigma$ , was calculated with eq 3

$$\sigma = \frac{t}{AR_{\text{ion}}} \tag{3}$$

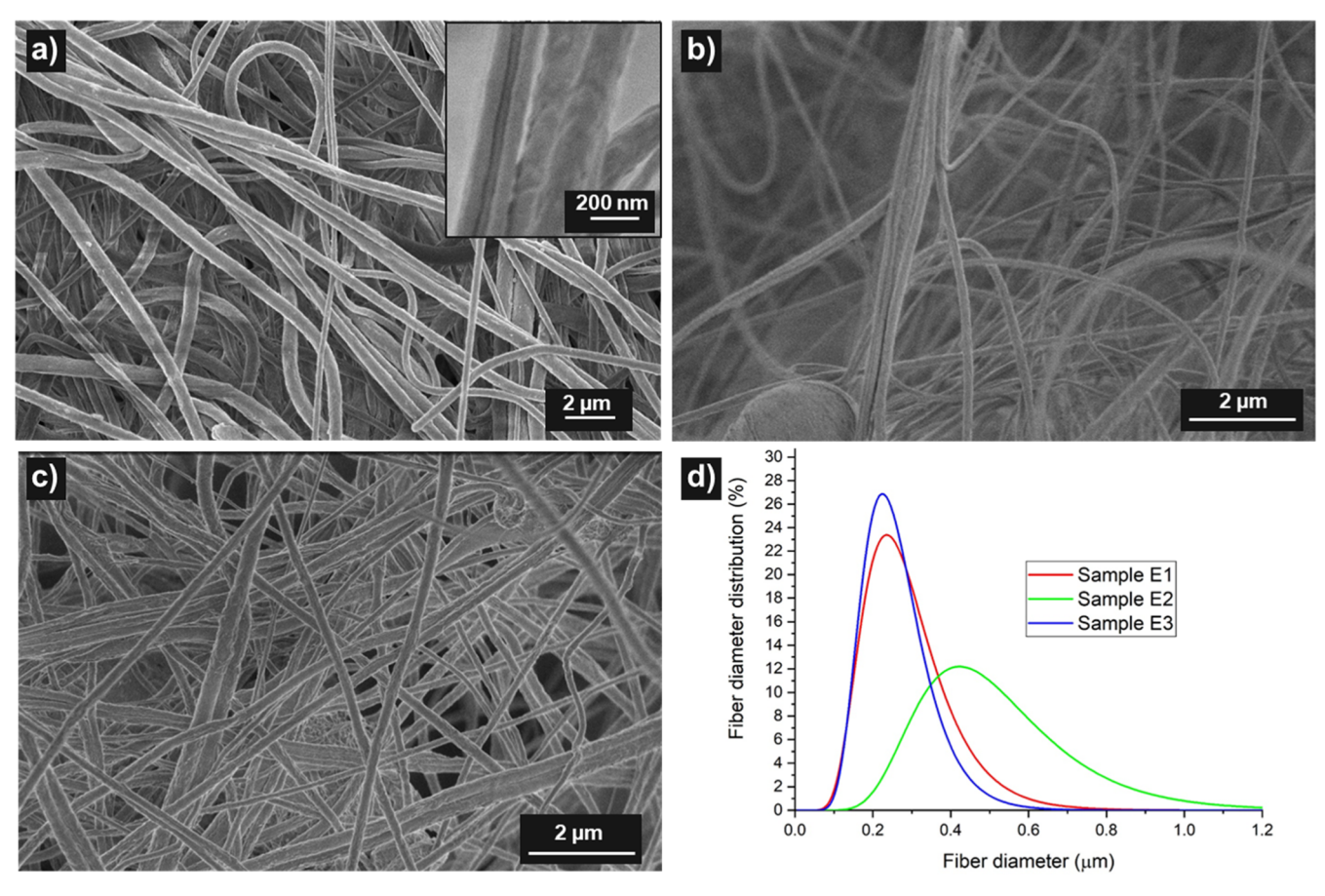


Figure 2. SEM images of electrospun PVDF separator E1 (a, with inset at higher magnification), E2 (b), and E3 (c) and resulting fiber diameter distributions (d).

where t is the membrane thickness,  $R_{\rm ion}$  is the measured ionic resistance (high-frequency intercept of Nyquist plot), and A is the membrane area.

Rate Capability and Cell Cycling Performance. Coin cells were assembled with a LiCoO $_2$  cathode (Electrodes and More, Richardson, TX) and a Li metal anode using a 1 M LiPF $_6$  EC/DMC (1:1 v/v), and chronopotentiometry measurements were performed with the VMP3 potentiostat. After conditioning the cells by cycling them between 3 and 4.20 V at a constant rate of C/20 for five cycles, they were then cycled at different C rates at room temperature. We refer to these experiments in the discussion section as rate capability measurements. Capacity is calculated as % of the first-cycle capacity, which corresponds to 100%. A minimum of three replicas per separator were assembled into coin cells and cycled to assess reproducibility.

# RESULTS AND DISCUSSION

Morphology and Fiber and Pore Distributions. In this section, we will compare the structure and membrane properties of samples prepared with the three different techniques highlighted in the experimental section.

Meltblown Membranes. Figure 1 shows scanning electron microscopy (SEM) images of representative meltblown PVDF mats prepared under the three processing conditions employed in this study and the corresponding distribution curve fits to the fiber diameters. The diameter of meltblown fibers is reported to be log-normally distributed, regardless of the mean fiber diameter. <sup>33–36</sup> However, the presence of a few large fibers in otherwise fine fibrous mats skews the distribution and increases their relative dispersity, leading to distributions that can be better approximated with normal curve fits. <sup>37</sup>

The fibers are smooth and featureless, but roping and entanglements of the fibers are present, especially evident with separator M1. The average fiber diameters are 1.7, 1.5, and 1.4  $\mu$ m for separators M1, M2, and M3, respectively, with size distributions spanning a few microns. Sample M1 is fabricated with high throughput and airflow, which produces the widest fiber size distribution with a standard deviation (SD) of 0.9 μm. Sample M3 is fabricated with a lower throughput (compared to separator M1) and produced a narrower size distribution with a slight decrease in fiber diameter. If polymer throughput and air flow are not well balanced in the meltblowing process, an instability of the melt exiting the die leads to fiber roping, entanglements, and a wide size distribution. A wide size distribution is not only easier to obtain, but it is also surprisingly beneficial for cycling stability, as we show later.

Electrospun Membranes. In comparison to meltblown fibers, the fibers in electrospun PVDF mats do not have as smooth a surface (Figure 2). The rapid evaporation of solvent during electrospinning is responsible for the small features visible on the fiber surface. The measured diameters of electrospun fibers were fit to log–normal distributions. The average fiber diameters are typically smaller (0.25–0.50  $\mu$ m) than those of meltblown mats (1.4–1.7  $\mu$ m). Separator E2 showed the largest average fiber diameter (0.51  $\mu$ m) among the electrospun separators with the broadest fiber size distribution. We suggest this distribution results from separator E2 using the highest PVDF concentration in the electrospinning solution; the resulting increased viscosity did not

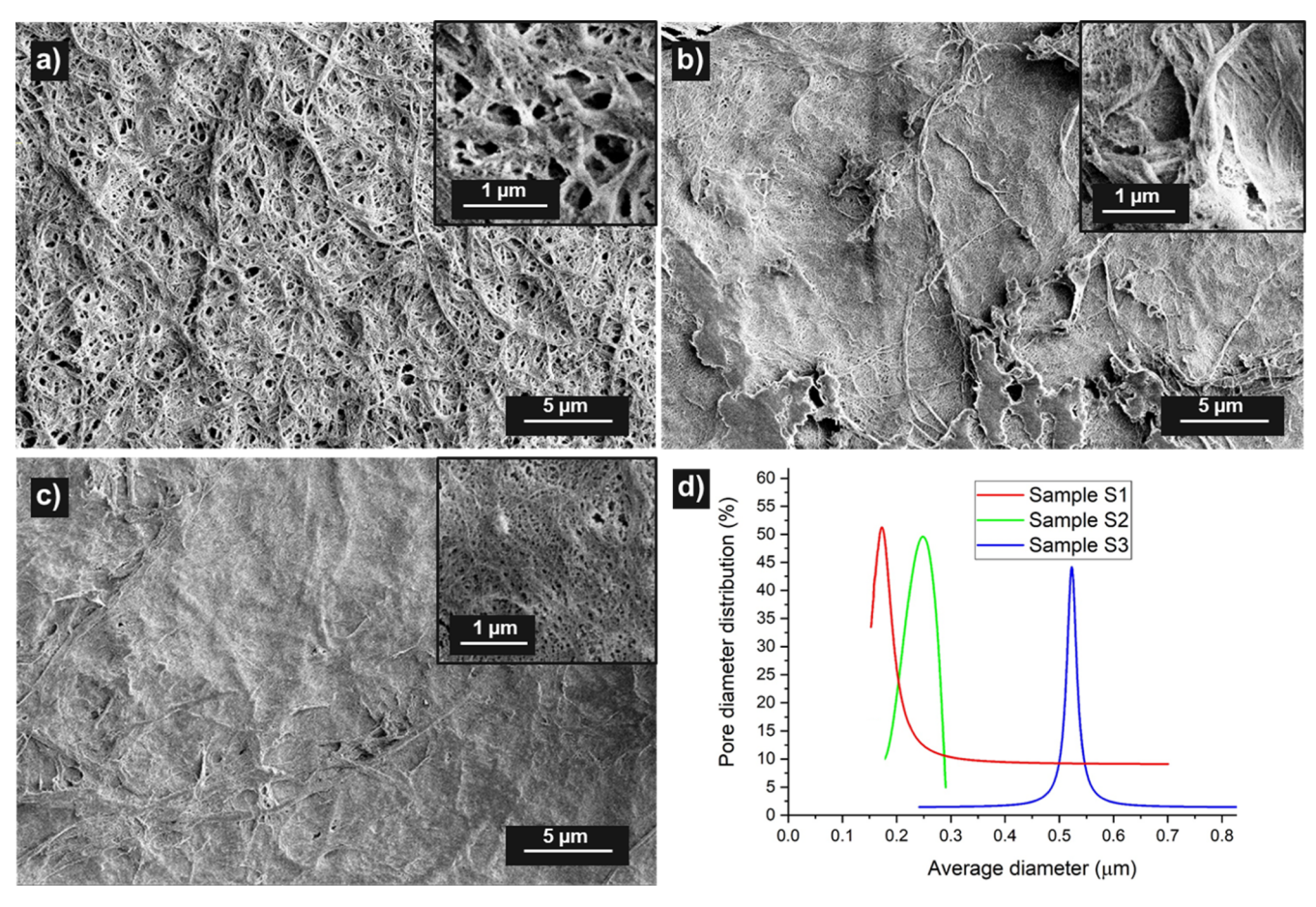


Figure 3. SEM images of SDC PVDF separator S1 (a, with the inset at higher magnification), S2 (b), and S3 (c) resulting pore diameter distributions (d).

Table 1. Solid Volume Percentage, Electrolyte Uptake, Ionic Conductivity, and Thickness of PVDF Separators Made by Meltblowing (M), Electrospinning (E), and Shear Spinning (S)

	M1	M2	M3	E1	E2	E3	S1	S2	S3
solid volume percent	18%	16%	18%	54%	27%	37%	23%	24%	33%
electrolyte uptake	740%	910%	705%	380%	475%	335%	325%	240%	235%
ionic conductivity (mS/cm)	4.34	6.91	5.61	0.47	2.00	0.29	1.21	0.56	0.51
thickness $(\mu m)$	115	175	140	110	150	200	20	23	27

allow the filaments to attenuate in diameter as much as in separators E1 and E3. On the other hand, separators E1 and E3 have similar average fiber diameters (0.26 and 0.29  $\mu m$ ), with separator E3 showing the narrowest distribution with only 0.08  $\mu m$  SD. In the electrochemical properties discussed below, we show that the combination of small average fiber diameter and wide diameter distribution is the most suitable structure for obtaining the highest cell cycling stability.

Shear-Spun Membranes. We have shown in previous work<sup>12</sup> that pore size is proportional to the fiber diameter comprising the mats. The shear-spun mats, however, do not always possess fibrous morphology, as discussed elsewhere.<sup>5</sup> Consequently, the comparison metric we employ here is pore size measured with capillary porosimetry, a technique more suitable to dense structures like shear-spun mats. SDC-based membranes differ from meltblown and electrospun mats because of their densely interconnected structure, as seen in Figure 3. The fibrous morphology is created with a low concentration (5%) of PVDF in the injection solution, which allows the SDC particles to branch out freely during formation

(Figure 3a).<sup>5</sup> At higher concentration (10%), the increased solution viscosity requires more energy to deform the polymer particles, leading to a mixed fibrous/NS morphology (Figure 3b). At 12.5% PVDF, the membranes are formed almost entirely with thin and highly porous NS particulates (Figure 3c).

Because the size of a SDC particles is not defined by one unique dimension (as they may comprise highly branched fibers, NSs, and mixtures thereof), the pore network may have a Gaussian, Lorentzian, or a mixed distribution. Here, the pore size data were fit to a Lorentzian distribution, as shown in Figure 3d. The SDC-based membranes have a uniform thickness with a continuous pore network, with pore sizes ranging from 10 to 500 nm. The NS particles assemble parallel to the membrane surface to create a spatially homogeneous and wide pore distribution [full width at half maximum, (fwhm) = 65 nm], but with an average pore size (250 nm) higher than that of SDC fibrous membranes (170 nm). The latter also present a broad pore size distribution (fwhm = 42 nm) despite the high number of pores below 200 nm. The

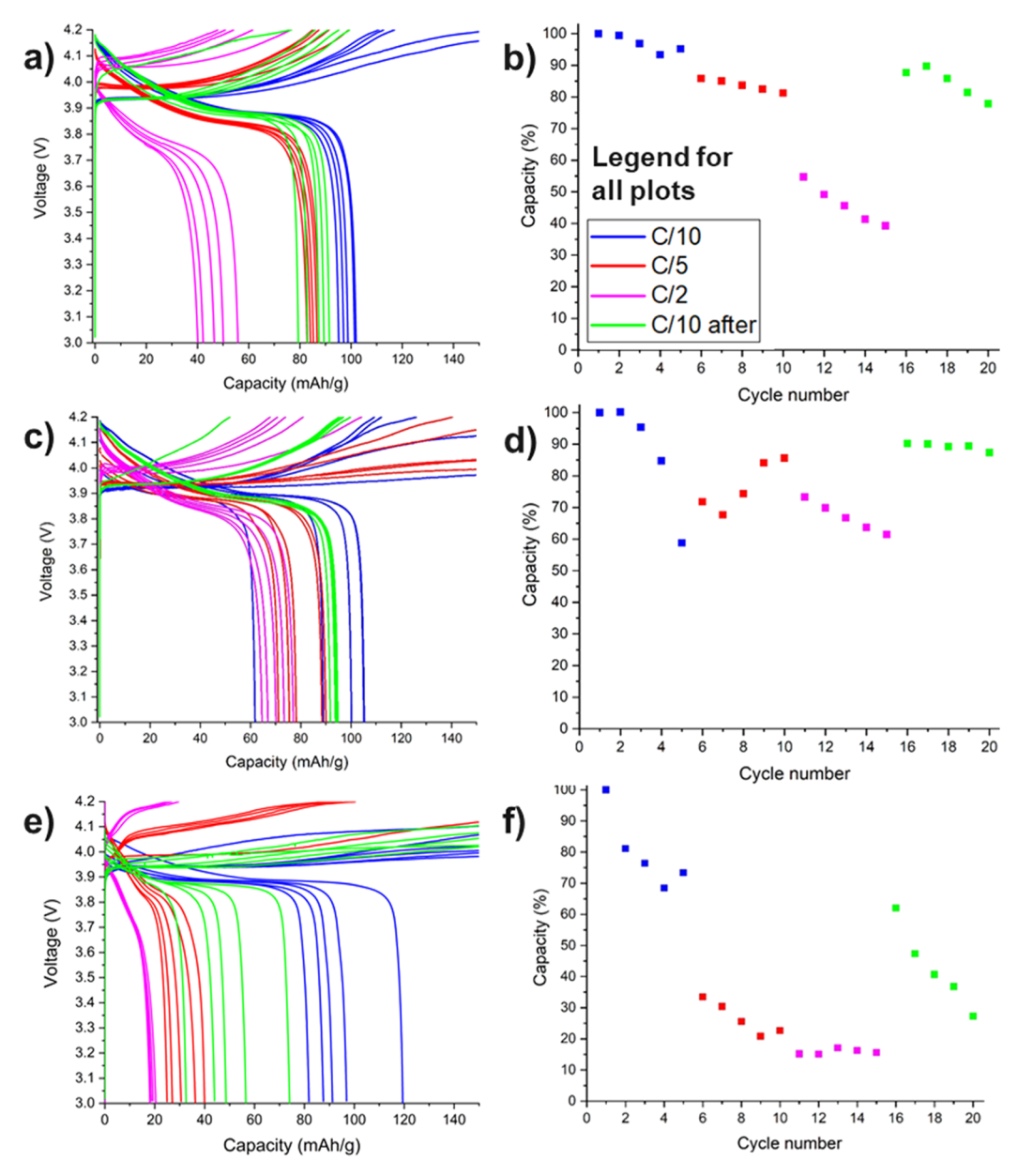


Figure 4. Charge-discharge curves and rate capability of cells containing meltblown PVDF separators M1 (a,b), M2 (c,d), and M3 (e,f).

fibrous-NS morphology membranes show a relatively narrow pore size distribution (fwhm = 22 nm) with large pore size (520 nm), which we attribute to a disrupted pore network caused by the combination of fibrous and NS morphologies.

**Electrochemical Properties.** In this section, we will compare the membrane properties (solid volume percent, electrolyte uptake, ionic conductivity, and thickness) of all separators. We will also analyze independently the cell cycling performance of separators each made with a different process, and we will correlate the performance of each separator to their membrane structure.

Meltblowing produces separators with the lowest solid volume percentage (<20%) among the three techniques used in our study (Table 1), followed by separators prepared by shear spinning (23–33%) and electrospinning (27–54%). The low solid volume percent is partly responsible for the high electrolyte uptake of meltblown separators (up to 910%). In addition, absorption of electrolyte in the outer surface of the PVDF fibers plays an important role. In previous studies, we

showed that the electrolyte modifies the morphology of the meltblown PVDF fibers by forming a gel-like structure on the outer surface of the mats, where the fibers are more amorphous. The Because shear-spun mats have a lower BW but a greater thickness than electrospun mats, the solid volume percent of electrospun and shear-spun mats is comparable. The lower the solid volume percent of a mat, the higher is its ionic conductivity, with meltblown separators having conductivities at least four times higher than shear-spun mats. We note that the higher the electrolyte uptake, the higher the conductivity for each set of separators (except separator M1, which may be because the spatial non-uniformity of the fibrous network did not enable a uniform volume expansion during electrolyte uptake).

Electrochemical stability of the separators is assessed by cycling Li-ion cells containing the PVDF mats at different C rates. Because the characteristics of the mats prepared with the three different processes do not allow a direct comparison between separators made with different techniques, we will

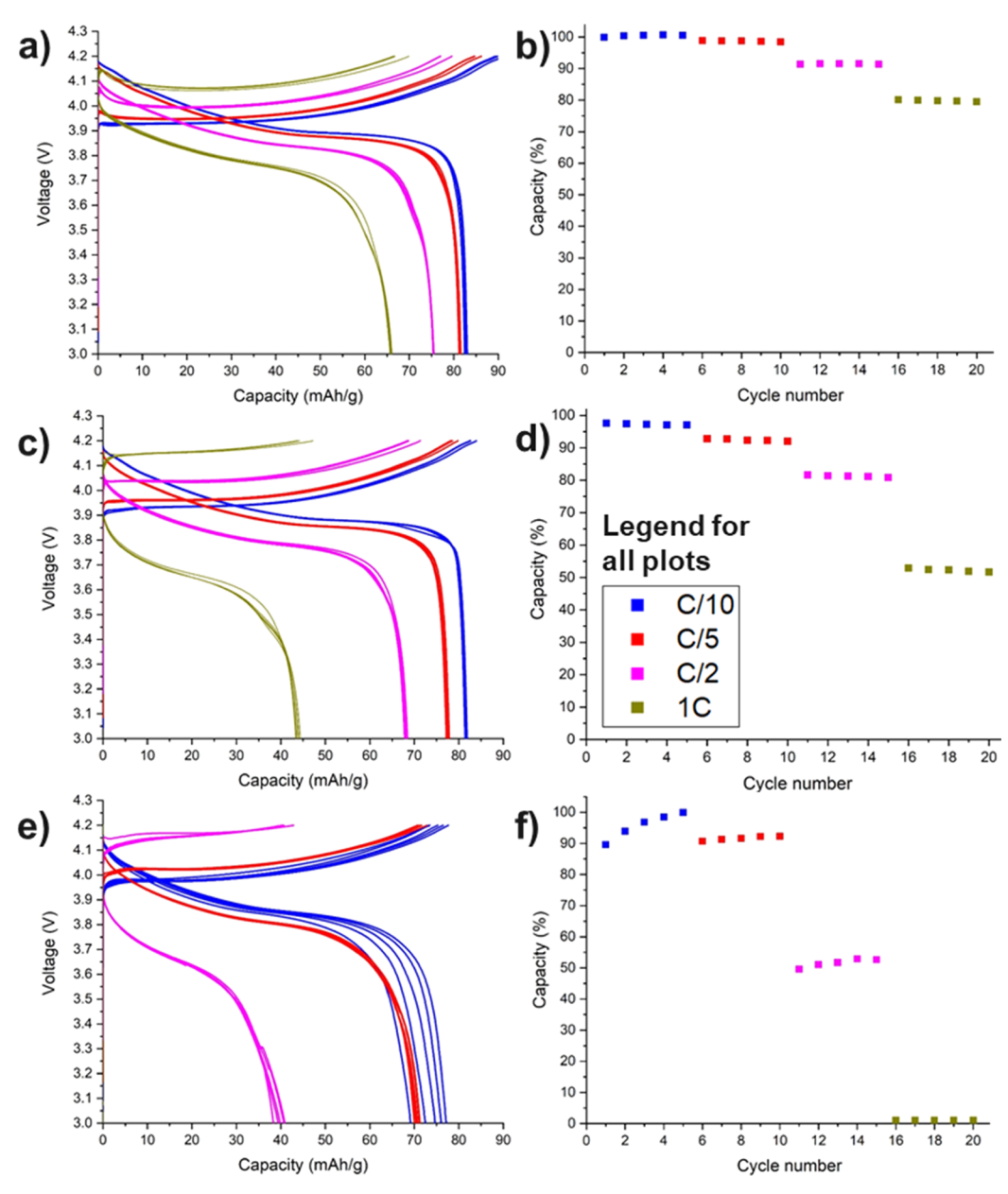


Figure 5. Charge-discharge curves and rate capability of cells containing electrospun PVDF separators E1 (a,b), E2 (c,d), and E3 (e,f).

discuss the effect that fiber/pore diameter and fiber/pore diameter distributions of the mats have on cell cycling performance when these mats are used as separators in Li/LiCoO $_2$  cells. The purpose of this discussion is to show that the fiber/pore diameter and fiber/pore diameter distribution of the mats have the same effect on fiber-based separators, independent of the process they are made of.

Meltblown Separators. Separator M1 has the widest diameter distribution among the meltblown mats, and it produces the best cycling performance in this set. Figure 4a,b shows that discharge capacity at C/10 and at C/5 rates varies less and capacity loss is reduced in cells employing meltblown separator M1 compared to cells with M2 (Figure 4c,d) and M3 (Figure 4e,f) mats. Sample M2 has a similar average fiber diameter compared to separator M3, but a wider diameter distribution, and it yields an improved cell cycling, with higher stability at high C rates and higher capacity retention after cycling (Figure 4c,d). As shown in Figure 4e,f, cells with

meltblown M3 separators show a significant change in capacity with the cycle number at low discharge rates (C/10) and significant capacity loss at higher discharge rates. Capacity retention after rate capability measurements is poor, and the cells have low Coulombic efficiencies (15-20%).

The only significant difference between cells containing M2 and M3 mats is the fiber diameter distribution. However, initial low-rate cycling of cells with separator M3 shows significant capacity loss, change in capacity with the cycle number, and low Coulombic efficiency (<20%). According to Table 1, thickness, ionic conductivity, electrolyte uptake, and solid volume percentage are similar between separators M1 and M3 and comparable with separator M2. Without other morphological differences, the distribution of fiber diameters is an effective factor influencing the cell behavior during cycling. Even though it may seem that a broader diameter distribution in the separator is advantageous for battery cycling stability, it is clear that even a small change in either the average fiber

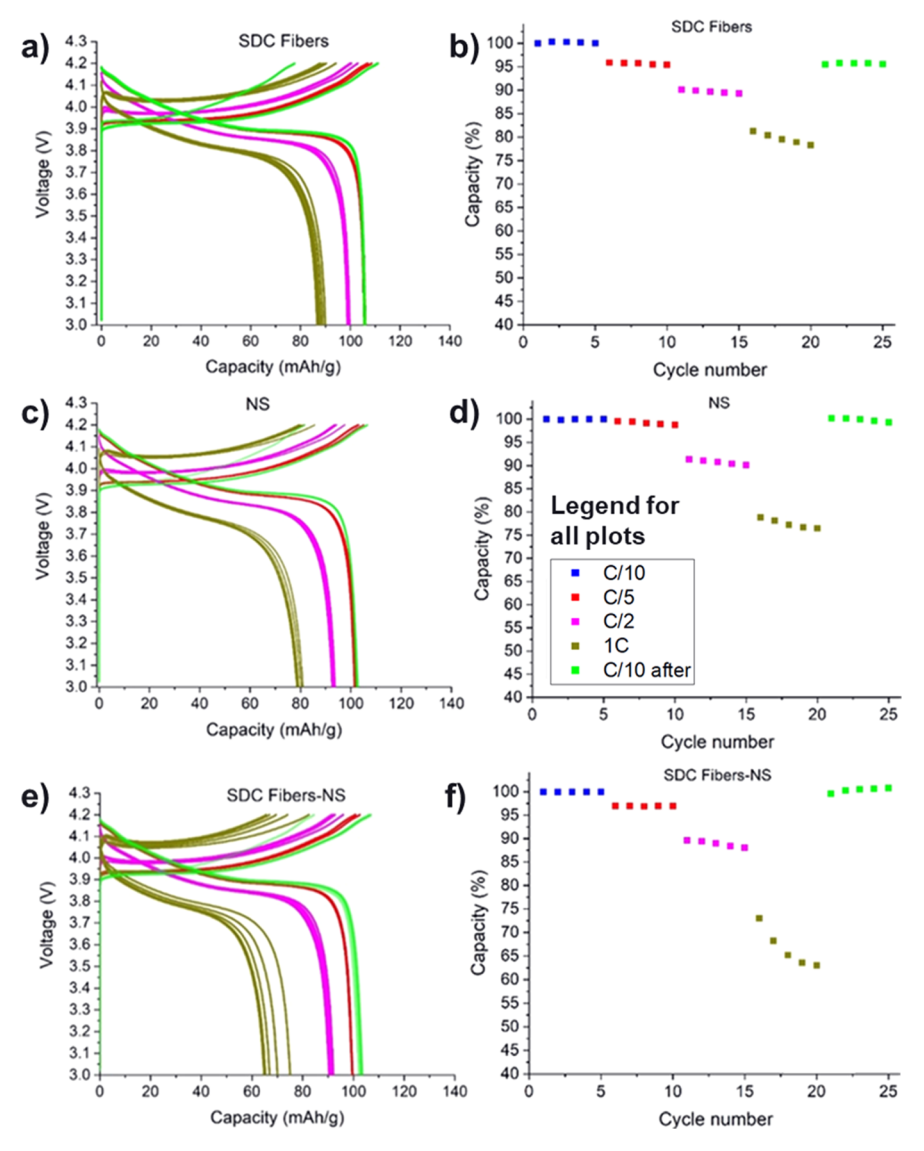


Figure 6. Charge—discharge curves and rate capability of cells containing SDC PVDF separators S1 (a,b), S2 (c,d), and S3 (e,f). Re-printed from (5), Copyright IoP Science.

diameter or its distribution will cause a significant change in performance. <sup>22–24</sup>

Electrospun Separators. Cells containing electrospun PVDF separators show better cycling performance than cells with meltblown separators (Figure 5). This trend may be explained by the smaller average fiber diameter for electrospun mats  $(0.25-0.50 \mu m)$  than those for meltblown separators  $(1.4-1.7 \mu m)$ , as shown in Figures 1 and 2. Separator E3 was fabricated at higher voltage (20 kV) than separators E1 and E2 (15 kV), which led to a narrower distribution in fiber diameter. Cells containing electrospun PVDF separators with narrow fiber size distributions show significant capacity variation with the cycle number and also capacity loss at rates higher than C/ 5 (Figure 5f). Separator E2 shows a wide diameter distribution and yields cells with stable cycling at all C rates, including 1C (not possible with separator E3). The capacity loss at low C rates is improved for both separators compared to that of separator E3. However, separator E2 not only shows a wide diameter distribution but also a large fiber diameter (0.51  $\mu$ m), double that of separator E1. Cells with separator E1 shows the best performance during cycling compared to cells employing

separators E2 and E3. Indeed, cells containing separator E1 showed little or no capacity loss at C/10 and C/5 and high and stable discharge capacity at all rates.

Table 1 shows that separators E1 and E3 have lower ionic conductivities than separator E2, which has the highest electrolyte uptake. Nonetheless, cells employing separator E1, which has the widest diameter distribution, show the highest capacity retention. However, solid volume percentage, mat thickness, and average fiber diameter affect electrolyte uptake and ionic conductivity, whose values are not necessarily reflected in cycling performance. For example, separators E1 and E3 have comparable uptake and conductivity but significantly different cycling performance. Similarly to meltblowing, the fiber diameter and its distribution for electrospun separators lead to changes in cycling performance. Low capacity variation with cycling and low capacity loss are achieved when the separator is fabricated with a low average fiber diameter (0.2–0.3  $\mu$ m) and a wide diameter distribution. However, as in the meltblowing case, separators E1 and E3 have a similar fiber distribution but provide significantly different cell performance, suggesting that when separators

have a similar fiber diameter, its distribution still plays a key role in the cell cycling performance.

Shear-Spun Separators. SDC-based membranes are beginning to be explored in electrochemical devices; to our knowledge, the present work is the first to evaluate their performance against other fiber separators. Because of the different characteristics of the mats, a direct comparison between cells containing meltblown, electrospun and shear-spun separators would not make sense. However, in all our experiments, the cell cycling performance of SDC separators was always more stable relative to electrospun or meltblown separators.

The S3 separators comprised a fibrous/NS mixed web. This morphology formed a homogeneous pore network with a large pore size (0.52  $\mu$ m) and narrow distribution (full-width half max = 22 nm), as shown in Figure 3. Separators with a narrow pore size distribution show higher capacity loss (in this case only at 1 C rate) than cells with separators with wide pore size distribution. Cells employing S2 separators with a NS morphology show improved stability compared to cells with S3 separators (mixed morphology), with little or no capacity loss at C/10 and at C/5 and stable 1C cycling. Cells employing the separator S1 with fibrous morphology show the highest stability and best performance, with a discharge capacity at C/10 of 106 mA h/g (vs M1 separator of 102 mA h/g and E1 separator of 86 mA h/g) and capacity loss at 1C equal to 18% (vs S2 separator of 23% and S3 separator of 35%) (Figure 6).

By employing one component (PVDF) and three different techniques to fabricate membranes, we are able to correlate the structural parameters of the separator mats to their electrochemical properties. Even with different grades of proportionality, similar conclusions may be drawn for each of the three different techniques used to fabricate separators. The fiber diameter or pore distribution has a major influence not only on the mat's physical and electrochemical properties, such as solid volume percentage, ionic conductivity, and electrolyte uptake, but also and more importantly on in-use cell-cycling stability and performance in a Li-ion cell. Meltblown separators had similar average fiber diameter, but the wider distribution of fiber diameters for separator M1, compared to separators M2 and M3, yielded a decreased capacity loss and improved cycling stability. Cells using the electrospun mats showed that a small average fiber diameter is not sufficient to yield high performance during cell cycling unless it is coupled with a wide fiber diameter distribution. Finally, when comparing shearspun separator S1 with separators S2 and S3, we see again that the combination of a wide diameter distribution and a small pore size lead to the best cell cycling performance, suggesting that a key factor in designing an optimal structure for a Li-ion battery separator is the combination of a small pore size and a wide pore size distribution, regardless of how the pore network is formed.

# CONCLUSIONS

By using three different techniques, meltblowing, electrospinning, and shear spinning, we fabricated PVDF Li-ion battery separators with variable fiber/pore diameters and pore size distributions. For a given processing technique, we adjusted the processing conditions to ensure that the main difference among the separators produced was the average fiber/pore diameter and size distribution. The separators prepared by the three techniques showed a similar trend when cycled in a Li-ion battery, that is, when the fiber/pore

distribution was widened and/or pore size was decreased, the capacity loss decreased and cycling stability increased. This effect was accentuated at C rates higher than C/5, suggesting that this specific separator structure is essential to enable high-rate cycling of Li-ion batteries. We also showed that shear spinning produces separators with a homogeneous and controlled structure, which combine a low solid volume percentage and low capacity losses with high cycling stability.

This work shows that by using a technique that fabricates homogeneous mats, separators may be produced with an optimal structure to improve the cycling performance of Li-ion batteries by designing the network with a small average pore size and a wide pore size distribution.

# AUTHOR INFORMATION

# **Corresponding Author**

Salvatore Luiso — Department of Chemical and Biomolecular Engineering, North Carolina State University, Raleigh, North Carolina 27695, United States; ⊚ orcid.org/0000-0002-9793-0444; Email: sluiso@ncsu.edu

#### Authors

Michael J. Petrecca – Department of Chemical and Biomolecular Engineering, North Carolina State University, Raleigh, North Carolina 27695, United States; orcid.org/ 0000-0002-7111-3526

Austin H. Williams – Department of Chemical and Biomolecular Engineering, North Carolina State University, Raleigh, North Carolina 27695, United States; orcid.org/ 0000-0003-4080-5164

Jerush Christopher – Department of Materials Science and Engineering, North Carolina State University, Raleigh, North Carolina 27695, United States

Orlin D. Velev – Department of Chemical and Biomolecular Engineering, North Carolina State University, Raleigh, North Carolina 27695, United States

Behnam Pourdeyhimi – The Nonwovens Institute, North Carolina State University, Raleigh, North Carolina 27695, United States

Peter S. Fedkiw — Department of Chemical and Biomolecular Engineering, North Carolina State University, Raleigh, North Carolina 27695, United States; orcid.org/0000-0003-4171-036X

Complete contact information is available at: https://pubs.acs.org/10.1021/acsapm.2c00216

#### **Author Contributions**

The article was written through contributions of all authors. All authors have given approval to the final version of the article.

#### Funding

This research was supported by the Nonwovens Institute (NWI), by NC State University, and by the US National Science Foundation CMMI-1825476.

#### Notes

The authors declare no competing financial interest.

# ■ ACKNOWLEDGMENTS

The authors gratefully acknowledge financial support from the US National Science Foundation, CMMI-1825476, and from North Carolina State University. We are thankful to Arkema, Inc., for their contribution to the material used in this work. We thank Brad Scroggins from the NWI pilot facility for

assistance with the meltblowing process. This work was performed in part at the Analytical Instrumentation Facility (AIF) at North Carolina State University, which is supported by the State of North Carolina and the National Science Foundation (award number ECCS-1542015). The AIF is a member of the North Carolina Research Triangle Nanotechnology Network (RTNN), a site in the National Nanotechnology Coordinated Infrastructure (NNCI).

# REFERENCES

- (1) Fu, Q.; Lin, G.; Chen, X.; Yu, Z.; Yang, R.; Li, M.; Zeng, X.; Chen, J. Mechanically Reinforced PVdF/PMMA/SiO<sub>2</sub> Composite Membrane and Its Electrochemical Properties as a Separator in Lithium-Ion Batteries. *Energy Technol.* **2018**, *6*, 144–152.
- (2) Pan, J.-L.; Zhang, Z.; Zhang, H.; Zhu, P.-P.; Wei, J.-C.; Cai, J.-X.; Yu, J.; Koratkar, N.; Yang, Z.-Y. Ultrathin and Strong Electrospun Porous Fiber Separator. ACS Appl. Energy Mater. 2018, 1, 4794–4803.
- (3) Li, M.; Liao, Y.; Liu, Q.; Xu, J.; Sun, P.; Shi, H.; Li, W. Application of the imidazolium ionic liquid based nano-particle decorated gel polymer electrolyte for high safety lithium ion battery. *Electrochim. Acta* **2018**, 284, 188–201.
- (4) Banerjee, A.; Ziv, B.; Shilina, Y.; Luski, S.; Halalay, I. C.; Aurbach, D. Multifunctional Manganese Ions Trapping and Hydro-fluoric Acid Scavenging Separator for Lithium Ion Batteries Based on Poly(ethylene- alternate -maleic acid) Dilithium Salt. *Adv. Energy Mater.* **2017**, *7*, 1601556.
- (5) Luiso, S.; Williams, A. H.; Petrecca, M. J.; Roh, S.; Velev, O. D.; Fedkiw, P. S. Poly(Vinylydene difluoride) Soft Dendritic Colloids as Li-Ion Battery Separators. *J. Electrochem. Soc.* **2021**, *168*, 020517.
- (6) Luiso, S.; Fedkiw, P. Lithium-ion battery separators: Recent developments and state of art. *Curr. Opin. Electrochem.* **2020**, 20, 99–107
- (7) Luiso, S.; Henry, J. J.; Pourdeyhimi, B.; Fedkiw, P. S. Meltblown PVDF as A Li-Ion Battery Separator. *ACS Appl. Polym. Mater.* **2021**, 3, 3038–3048.
- (8) Huang, X. Separator technologies for lithium-ion batteries. *J. Solid State Electrochem.* **2011**, *15*, 649–662.
- (9) Venugopal, G.; Moore, J.; Howard, J.; Pendalwar, S. Characterization of microporous separators for lithium-ion batteries. *J. Power Sources* **1999**, *77*, 34–41.
- (10) Djian, D.; Alloin, F.; Martinet, S.; Lignier, H.; Sanchez, J. Y. Lithium-ion batteries with high charge rate capacity: Influence of the porous separator. *J. Power Sources* **2007**, *172*, 416–421.
- (11) Kim, J. Y.; Lim, D. Y. Surface-modified membrane as a separator for lithium-ion polymer battery. *Energies* **2010**, *3*, 866–885.
- (12) Luiso, S.; Henry, J. J.; Pourdeyhimi, B.; Fedkiw, P. S. Fabrication and Characterization of Meltblown Poly(vinylidene difluoride) Membranes. ACS Appl. Polym. Mater. 2020, 2, 2849–2857.
- (13) Luo, R.; Wang, C.; Zhang, Z.; Lv, W.; Wei, Z.; Zhang, Y.; Luo, X.; He, W. Three-Dimensional Nanoporous Polyethylene-Reinforced PVDF-HFP Separator Enabled by Dual-Solvent Hierarchical Gas Liberation for Ultrahigh-Rate Lithium Ion Batteries. *ACS Appl. Energy Mater.* **2018**, *1*, 921–927.
- (14) Liu, J.; Shi, X.; Boateng, B.; Han, Y.; Chen, D.; He, W. A Highly Stable Separator from an Instantly Reformed Gel with Direct Post-Solidation for Long-Cycle High-Rate Lithium-Ion Batteries. *Chem-SusChem* **2019**, *12*, 908–914.
- (15) Ye, L.; Shi, X.; Zhang, Z.; Liu, J.; Jian, X.; Waqas, M.; He, W. An Efficient Route to Polymeric Electrolyte Membranes with Interparticle Chain Microstructure Toward High-Temperature Lithium-Ion Batteries. *Adv. Mater. Interfaces* **2017**, *4*, 1–6.
- (16) Liu, B.; Huang, Y.; Zhao, L.; Huang, Y.; Song, A.; Lin, Y.; Wang, M.; Li, X.; Cao, H. A novel non-woven fabric supported gel polymer electrolyte based on poly(methylmethacrylate-polyhedral oligomeric silsesquioxane) by phase inversion method for lithium ion batteries. *J. Membr. Sci.* **2018**, *564*, 62–72.

- (17) Wang, X.; Xu, G.; Wang, Q.; Lu, C.; Zong, C.; Zhang, J.; Yue, L.; Cui, G. A phase inversion based sponge-like polysulfonamide/SiO<sub>2</sub> composite separator for high performance lithium-ion batteries. *Chin. J. Chem. Eng.* **2018**, 26, 1292–1299.
- (18) Li, Y.; Li, Q.; Tan, Z. A review of electrospun nanofiber-based separators for rechargeable lithium-ion batteries. *J. Power Sources* **2019**, 443, 227262.
- (19) Waqas, M.; Ali, S.; Feng, C.; Chen, D.; Han, J.; He, W. Recent Development in Separators for High-Temperature Lithium-Ion Batteries. *Small* **2019**, *15*, 1901689.
- (20) Lee, Y.; Park, J.; Jeon, H.; Yeon, D.; Kim, B.-H.; Cho, K. Y.; Ryou, M.-H.; Lee, Y. M. In-depth correlation of separator pore structure and electrochemical performance in lithium-ion batteries. *J. Power Sources* **2016**, 325, 732–738.
- (21) Ye, W.; Zhu, J.; Liao, X.; Jiang, S.; Li, Y.; Fang, H.; Hou, H. Hierarchical three-dimensional micro/nano-architecture of polyaniline nanowires wrapped-on polyimide nanofibers for high performance lithium-ion battery separators. *J. Power Sources* **2015**, 299, 417–424
- (22) Sabetzadeh, N.; Gharehaghaji, A. A.; Javanbakht, M. Porous PAN micro/nanofiber separators for enhanced lithium-ion battery performance. *Solid State Ionics* **2018**, *325*, 251–257.
- (23) Jiang, Y.; Ding, Y.; Zhang, P.; Li, F.; Yang, Z. Temperature-dependent on/off PVP@TiO<sub>2</sub> separator for safe Li-storage. *J. Membr. Sci.* **2018**, *565*, 33–41.
- (24) Zhai, Y.; Wang, N.; Mao, X.; Si, Y.; Yu, J.; Al-Deyab, S. S.; El-Newehy, M.; Ding, B. Sandwich-structured PVdF/PMIA/PVdF nanofibrous separators with robust mechanical strength and thermal stability for lithium ion batteries. *J. Mater. Chem. A* **2014**, *2*, 14511–14518.
- (25) International Organization for Standardization. (2003). Paper and board Determination of air permeance and air resistance (medium range) Part 5: Gurley method (ISO Standard No. 5636-5). Retrieved from https://www.iso.org/standard/37376.html (accessed April 03, 2022).
- (26) Velev, O. D., Smoukov, S., Geisen, P., Wright, M. C., Gangwal, S. Method for Fabricating Nanofibers. U.S. Patent 9,217,211 B2, 2015.
- (27) Velev, O., Smoukov, S., Marquez, M. Nanospinning of polymer fibers from sheared solutions. U.S. Patent 8,551,378 B2, 2015.
- (28) Roh, S.; Williams, A. H.; Bang, R. S.; Stoyanov, S. D.; Velev, O. D. Soft dendritic microparticles with unusual adhesion and structuring properties. *Nat. Mater.* **2019**, *18*, 1315–1320.
- (29) Henry, J. J.; Goldbach, J.; Stabler, S.; Devisme, S.; Chauveau, J. Advancements in the production of meltblown fibres. *Filtr. Sep.* **2016**, 53, 36–40.
- (30) Henry, J. J., Goldbach, J., Stabler, S., Chauveau, J. High melt flow fluoropolymer composition. U.S. Patent 20,170,088,989 A1, 2017.
- (31) Reifenhauser REICOFIL Meltblown Pilot Line, Available from: https://thenonwovensinstitute.com/wp-content/uploads/2015/04/Reifenhauser-Reicofil-Meltblown-Pilot-Brochure.pdf (accessed 04/03/2022).
- (32) Jena, A.; Gupta, K. Liquid extrusion techniques for pore structure evaluation of nonwovens. *Int. Nonwovens J.* **2003**, *os-12* (3), 45–53.
- (33) Yarin, A. L.; Sinha-Ray, S.; Pourdeyhimi, B. "Meltblowing: Multiple polymer jets and fiber-size distribution and lay-down patterns,". *Polymer* **2011**, *52*, 2929–2938.
- (34) Wang, X.; Ke, Q. Experimental Investigation of Adhesive Meltblown Web Production Using Accessory Air. *Polym. Eng. Sci.* **2006**, *46*, 1–7.
- (35) Tan, D. H.; Zhou, C.; Ellison, C. J.; Kumar, S.; Macosko, C. W.; Bates, F. S. Meltblown fibers: Influence of viscosity and elasticity on diameter distribution. *J. Nonnewton. Fluid Mech.* **2010**, *165*, 892–900. (36) Ellison, C. J.; Phatak, A.; Giles, D. W.; Macosko, C. W.; Bates, F. S. Melt blown nanofibers: Fiber diameter distributions and onset of fiber breakup. *Polymer* **2007**, *48*, 3306–3316.

- (37) Barilovits, S. "Experimental Study of a Unique Multi-Row Meltblowing Fiber Formation Process and the Web Structures Produced Thereby". Ph.D. Thesis, NC State Repository, 2018.
- (38) Tan, A. R.; Ifkovits, J. L.; Baker, B. M.; Brey, D. M.; Mauck, R. L.; Burdick, J. A. Electrospinning of photocrosslinked and degradable fibrous scaffolds. *J. Biomed. Mater. Res.* **2008**, 87A, 1034—1043.
- (39) Malašauskienė, J.; Milašius, R. Mathematical Analysis of the Diameter Distribution of Electrospun Nanofibres. *Fibres Text. East. Eur.* **2010**, *18*, 45–48.
- (40) Petrakis, D. E.; Hudson, M. J.; Sdoukos, A. T.; Pomonis, P. J.; Bakas, T. B. Controlled modulation of mesoporosities in metal (M = Al, Fe) phosphate solids. *Colloids Surf., A* **1994**, *90*, 191–202.

# **□** Recommended by ACS

Nanostructured Ionic Separator Formed by Block Copolymer Self-Assembly: A Gateway for Alleviating Concentration Polarization in Batteries

Xiaopeng Yu, Nitash P. Balsara, et al.

MARCH 28, 2022 MACROMOLECULES

READ **Z** 

3D Fiber-Network-Reinforced Bicontinuous Composite Solid Electrolyte for Dendrite-free Lithium Metal Batteries

Dan Li, Li-Zhen Fan, et al.

FEBRUARY 07, 2018

ACS APPLIED MATERIALS & INTERFACES

READ 🗹

Transport Properties of Flexible Composite Electrolytes Composed of Li1.5Al0.5Ti1.5(PO4)3 and a Poly(vinylidene fluoride-co-hexafluoropropylene) Ge...

Ji-young Ock, Kaoru Dokko, et al.

JUNE 09, 2021 ACS OMEGA

READ 🗹

"Salt-in-Fiber" Electrolyte Enables High-Voltage Solid-State Supercapacitors

Loujain G. Ghanem, Nageh K. Allam, et al.

MAY 10, 2022

ACS APPLIED ENERGY MATERIALS

READ 🗹

Get More Suggestions >